Front. Earth Sci. 2024, 18(3): 671−682
https://doi.org/10.1007/s11707-024-1110-5

RESEARCH ARTICLE

Sedimentary architecture of a sandy braided river with seasonal hydrodynamic variations: insights from the Permian Lower Shihezi Formation, Ordos Basin, China

Xiaohui LI (✉)[1,2], Yuliang SU[1], Guanglei REN[2], Feixiang GAO[1,2], Shuhong YAN[2], Huachao SUN[2], Hui RAN[2], Mengdi CUI[2]

1 School of Petroleum Engineering, China University of Petroleum (East China), Qingdao 266000, China
2 Research Institute of Exploration and Development, Sinopec North China Petroleum Bureau, Zhengzhou 450000, China

Abstract A sandy, braided river is a typical type of river that exists in ancient and modern alluvial plains and is inherent with significant seasonal water discharge variations. The variations play an important role in the depositional process and the formation of the sedimentary architecture of braided rivers. In this paper, a braided river outcrop along the Yellow River in Fugu is used to describe the effects of seasonal hydrodynamic variations on braided river sedimentary architecture. The results show that the braided channel network exhibits two different patterns during flood period and normal period. During flood periods, the main braided channels surrounding channel bars and the secondary braided channels distributed on the top of the channel bars coexist, forming a highly braided channel network. Migration of the main braided channels control the formation of middle channel bars and side bars. The generation and evolution of the secondary braided channels reformed the upper part of preexisting channel bars and produced affiliated bars along their flow path. During the normal period, water levels decrease, causing the secondary river channels to be abandoned and forming abandoned channels, and only the main braided channels stay active. In the long term sedimentation process, strong water flow during the flood period continuously erodes pre-existing sediments and forms new sediments, while weak water flow during the normal period can only reform the main braided channels and their adjacent channel bar sediments. Based on differences in sedimentary processes and associated hydrodynamic conditions, braided river sediments are divided into two combinations. The strong hydrodynamic combination includes main braided channels, middle channel bar, and side bar, while the weak hydrodynamic combination includes secondary braided channels, abandoned channels, and affiliated bars. The proportion of strong hydrodynamic combinations is much larger than that of weak hydrodynamic combinations. Based on this, we construct a braided river sedimentary architecture model that is helpful for the fine characterization of subsurface oil and gas reservoirs.

Keywords sandy-braided river, Ordos Basin, Lower Shihezi Formation, seasonal hydrodynamic variations, sedimentary architecture

1 Introduction

Sandy-braided river deposits are common throughout the ancient stratigraphic record (Allen, 1983; Bridge et al., 1986; Bridge and Tye, 2000; Bridge, 2003; Cain and Mountney, 2009). Modern braided rivers mostly develop in tropics and subtropics, and are affected by seasonal hydrodynamic variations (Mosley, 1983; Vandenberghe, 1995; Fielding et al., 2009; Plink-Björklund, 2015; Wang et al., 2023). Water discharge rates tend to rise and fall dramatically with changing seasons, mostly showing low-energy in normal periods, and high-energy in the flood periods (Ashworth et al., 2000; Best et al., 2003; Cain and Mountney, 2009). Recent studies of modern river systems show that braided rivers formed under seasonal hydrodynamic variations possess unique, depositional properties, including: 1) erosionally based channel-fill lithosomes that exhibit complex lateral facies changes, with 2) abundant, pedogenically modified mud partings, 3) complex internal architecture that may lack the typical macroform elements of other fluvial sediment bodies, 4) an abundance of sedimentary structures formed under high

Received August 18, 2023; accepted November 19, 2023

E-mail: oilgasfieldlixh@163.com

flow stage, and 5) an abundance of in situ trees that colonize channel floors and are adapted to inundation by fast-flowing water (Fielding et al., 2009, 2018; Plink-Björklund, 2015). Seasonal hydrodynamic variations and associated sediment transport variations control the depositional process, sedimentary structures and internal architecture. For example, there is significant difference between the channel network and its braiding intensity in the normal and flood periods (Smith, 1974; Bluck, 1979; Carson, 1984; Gupta and Dutt, 1989; Li et al., 2020; Gao et al., 2022; You et al., 2022). Secondly, the sediment that already exists on the surface of the riverbed will frequently undergo erosion and transformation, resulting in low preservation of sediment structures formed during normal and flood periods, as well as a complex internal architecture typically seen with braided rivers (Doeglas, 1962; Miall, 1977b; Blodgett and Stanley, 1980; Ashmore, 1982, 1991; Skelly et al., 2003; Fielding et al., 2009; Plink-Björklund, 2015). Additionally, sediments deposited in normal and flood periods coexist in preserved braided river deposits (Krigström, 1962; Coleman, 1969; Collinson, 1970; Smith, 1970; Cant and Walker, 1978; Bridge et al., 1986; Bristow, 1987).

Although there has been extensive research on the sedimentary characteristics of braided rivers, these studies are primarily based on the observation of modern rivers and the analysis of shallow trenches (Doeglas, 1962; Cant and Walker, 1978; Fielding et al., 2009, 2018; Plink-Björklund, 2015; Li et al., 2020; Gao et al., 2022; You et al., 2022), which cannot fully reveal the sedimentary characteristics and sedimentary architecture patterns preserved in stratigraphic records. However, systematic and detailed sedimentary characteristics and sedimentary architecture patterns are crucial for characterizing subsurface oil and gas reservoirs.

In this paper, a typical outcrop of a sandy-braided river formed under seasonal hydrodynamic variation conditions was investigated. Depositional units, including lithofacies and architecture elements formed under strong and weak hydrodynamics, were recognized, and a detailed sedimentary architecture model of the braided river was constructed for subsurface reservoir forecasting.

2 Geological settings

In the Early-Middle Permian, the Ordos Basin was a typical depression basin with a wide gentle slope dipping from north to south (Li et al., 2021). Sediment transported from the northern Yinshan Mountains and formed a large alluvial plain on the gentle slope, oriented near north–south (Chen et al., 2009). During deposition of the Middle Permian Lower Shihezi Formation, braided rivers were widely distributed on the gentle slope and formed a sandy-braided river sequence in the northern Ordos Basin (Yang et al., 2004; Wen et al., 2007; Chen et al., 2019; Li et al., 2021). After subsequent complex tectonic movements, these strata are well exposed in Fugu County, Yulin City, Shaanxi Province, China (Fig. 1(a)) and outcrops under the Tianshengqiao viaduct (Fig. 1(b)). The stratum exposed in this outcrop is the lowermost member (member He8) of the Lower Shihezi Formation (Fig. 1(c)), which has an overall thickness of about 50 m, and can be further divided into 4 layers (He8-1 to He8-4). Various sedimentary structures of braided river deposits can be recognized from the outcrop, such as parallel or planar laminations, tabular cross bedding, etc. Braided channels and channel bars can also be directly observed (Chen et al., 2019). The whole outcrop consists of two perpendicular sections (Fig. 1(b) section A-B and section C–J) and one isolated section nearly parallel to the section C–J (Fig. 1(b) section G–H). The total length of the outcrop is 1400 m. The strike of profiles A–B, C–J, and G–H are 37°, 300°, and 311°, respectively, and are oblique to the paleocurrent direction (Fig. 1).

3 Data and methodology

3.1 Data collection and outcrop model construction

To systematically analyze the sedimentary architecture of the braided river, we utilized an unmanned aerial vehicle (DJI-M300 RTK) to take oblique photography of the target outcrop, and further used DJI Terra software to establish a high-precision 3D model of the outcrop. The model provides a full range of imagery and spatial information for outcrops with sub-centimeter accuracy (Figs. 1 and 2). In addition, we conducted detailed observations, photography, and sediment particle size measurements on the accessible parts of the outcrop.

3.2 Methodology for sedimentary architecture analysis

Based on the model, we identified and tracked architectural boundaries on the outcrop, identified sedimentary structures, and preliminarily analyzed the lithology and grain size. Through lithofacies identification, lithofacies association analysis, sedimentary elements observation and hierarchical surface boundary tracking, the outcrop braided river sedimentary architecture was investigated.

4 Lithofacies

During fluvial deposition, diverse hydrodynamic conditions and sediment transport processes lead to the formation of a variety of lithofacies with different grain sizes, sedimentary structures, and scales (Miall, 1977a, 1977b, 2013). Each type of lithofacies has a certain genetic condition. Therefore, identifying lithofacies is considered to be a necessary prerequisite for sedimentary architecture analysis.

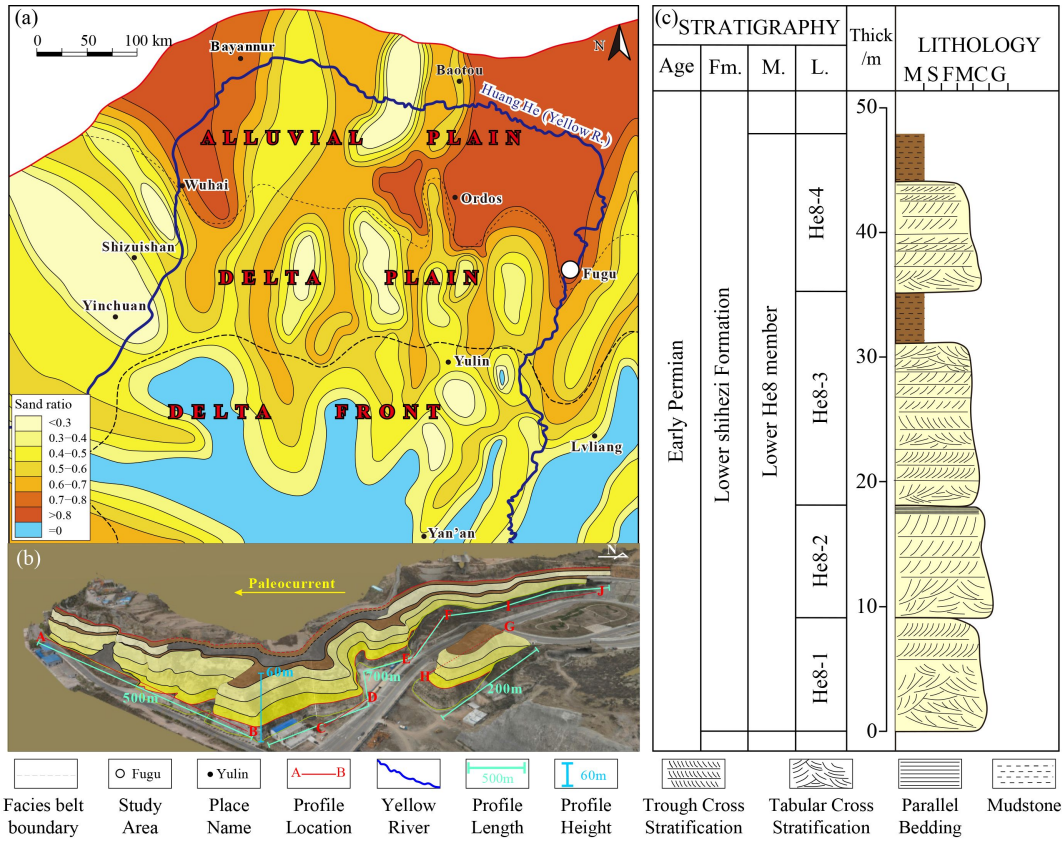

Fig. 1 (a) Sedimentary facies diagram of Lower Shihezi Formation in Ordos Basin. (b) Digital Outcrop Model and formation exposure of He8 member. The outcrop is about 1400 m, and the stratum slope is 4°. The outcrop was divided into 3 long profiles (A-B, C-J, and G-H). (c) Stratigraphic framework of He8 member. M. means member unit, L. means layer unit within a member unit. The text in (c) marked from left to the right as M, S, F, M, C, and G means mud, silt, fine sand, medium sand, coarse sand, and gravel sediments.

In this paper, nine lithofacies were recognized from the outcrop (Fig. 3), including two types of massive sandy conglomerate, parallel bedded sandstone, two types of trough cross-stratification sandstone, two types of tabular cross-stratification sandstone, massive sandstone, and massive mudstone (Table 1). Moreover, there is a distinct variation in scale and distribution of massive, sandy conglomerates, trough cross-stratification and tabular cross-stratification, which indicates that the corresponding hydrodynamics in deposition is quite different. Therefore, they are classified into several sub-lithofacies based on the scale and distribution of the primary lithofacies.

4.1 Massive, sandy conglomerate

Massive-sandy conglomerates can be classified into two types (Gm1 and Gm2). GM1 is generally distributed at the bottom of channel deposits, with a thickness of 0.2−1.0 m. Gravel particles have a diameter of 0.2 to 1.5 cm and can be interpreted as lag deposits formed under strong hydrodynamics (Fig. 3(a)). Gm2 is distributed in the lower part of the thick sand body with a thickness of 0.5−2.0 m, with gravel particles 0.5−1.0 cm in diameter (Fig. 3(b)) and can be interpreted as large-scale channel fill deposits. Although Gm2 is not a lag deposit, the hydrodynamics are stronger than that of Gm1. Both types of sub-lithofacies are the products of channel filling and can be commonly observed on the outcrop.

4.2 Parallel bedded sandstone

Parallel bedded sandstones (Sh) are commonly observed on the outcrop, with grain size ranging from medium sand to coarse. The thickness of a single Sh unit is 0.3−0.5 m, and multiple Sh units are often superimposed to form a thick sand body several meters thick (Fig. 3(c)). Sh is the most abundant lithofacies that occurs in the middle to upper part of thick sand bodies and is interpreted as channel bar deposits. The Sh belongs to a typical Froude transcritical and supercritical flow sedimentary structure. According to the observation, Sh accounts for over 70% of the area on the entire outcrop.

4.3 Trough cross-bedded sandstone

Trough cross-bedded sandstone (St) is also common on the outcrop. According to the scale and distribution, St

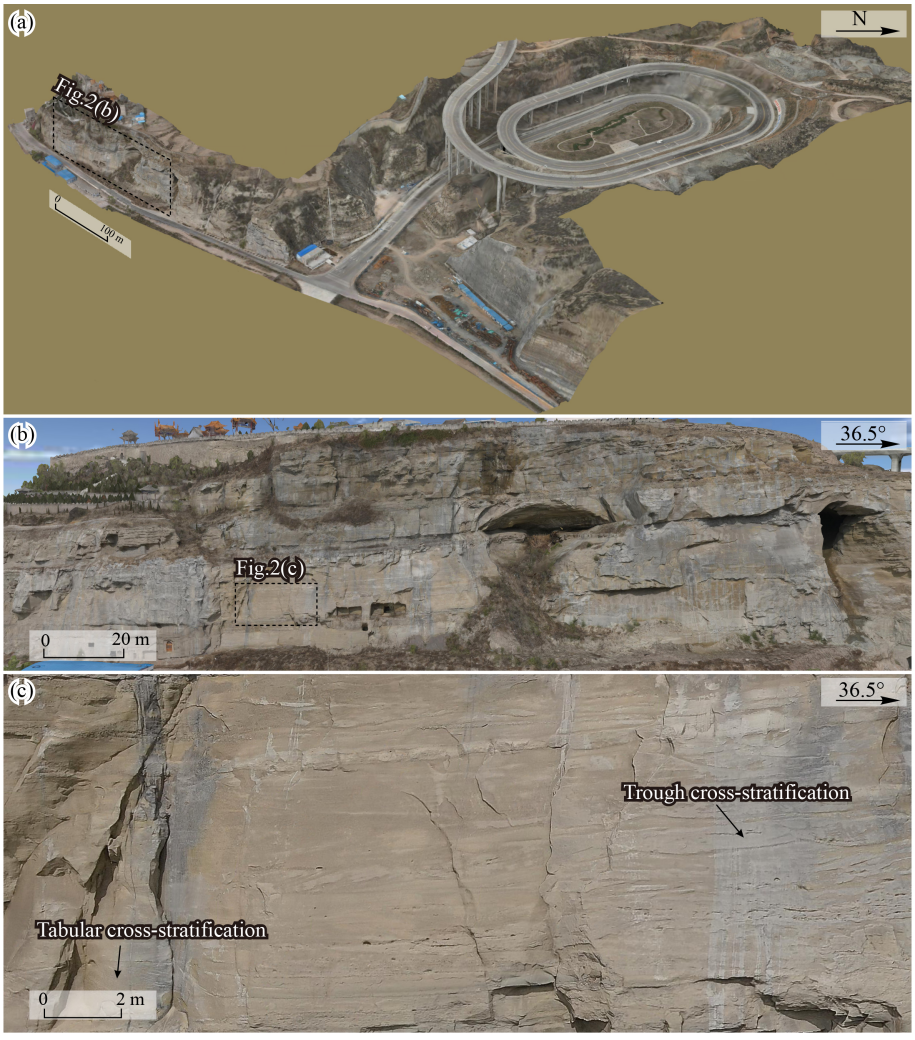

Fig. 2 The whole view of the Tianshengqiao outcrop (a), the A-B profile of the outcrop (b) and the partial image of the A-B profile. The boundaries of the architectural elements at different levels and the sedimentary structures inside the architectural elements are clearly observed.

can be divided into two types (St1 and St2). The scale of St1 is relatively large, with a width of several meters and a thickness of more than 1 m. The sediments are mainly medium-coarse sand, which are generally distributed in the middle and lower parts of large braided channels (Fig. 3(d)). In contrast, the scale of St2 is small, and the sediments are mostly medium-sand, generally less than 1m in width and 20−40 cm in thickness, distributed in small braided channels (Fig. 3(e)). The two sub-litho-facies indicate that relatively strong and weak hydrodynamic conditions generally existed during the deposition of braided channels.

4.4 Tabular cross-bedded sandstone

Tabular cross-bedded sandstone mostly occurs in the sandy bed, and the sediment composition is generally well-sorted medium sand, which is formed on the open and flat bed. The thickness of Sp depends on the water depth and hydrodynamic strength at the time of deposition. According to the thickness of Sp, it can be divided into two types (Sp1 and Sp2). Sp1 usually has a thickness of more than 0.4 m and a width of up to tens of meters (Figs. 3(f) and 3(g)). The sediments are mainly medium-coarse sand. Multiple SP1 units stacked vertically can be more than 8 m thick. Compared with SP1, the thickness of SP2 is generally only about 0.2 m, and the sediment grain size is also finer (medium to fine sand).

4.5 Massive sandstone

Massive sandstone is generally distributed in large-scale thick sandstone of channel bars, generally medium sandstone, sediments are well sorted (Fig. 3(h)). Its thickness can generally reach 2−15 m. This lithofacies can be interpreted as channel bar deposit formed under strong hydrodynamic conditions.

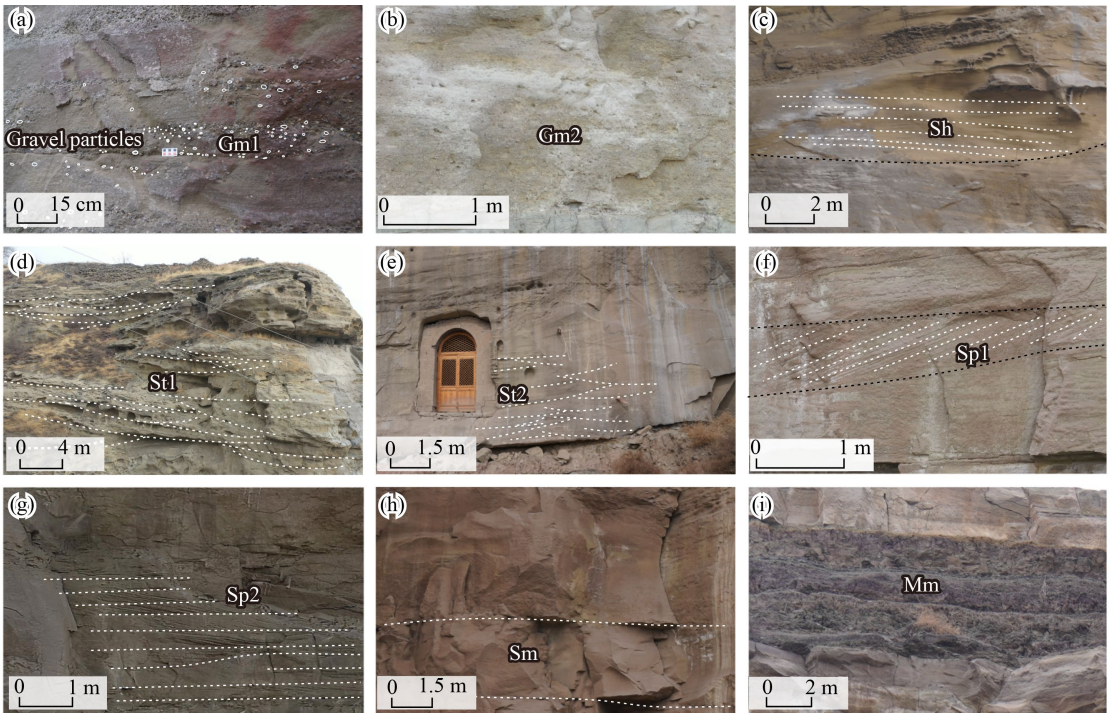

Fig. 3 Typical lithofacies types of braided river deposits of He8 member. (a−b) Massive sandy conglomerate (Gm1 and Gm2); (c) parallel bedded sandstone (Sh); (d−e) trough cross-stratification sandstone (St1 and St2); (e) small trough cross-stratification sandstone (St2); (f−g) tabular cross-stratification sandstone (Sp1 and Sp2); (h) massive sandstone (Sm); (i) massive mudstone (Mm).

Table 1 Summary of the characteristics of lithofacies observed on the Tianshengqiao outcrop

Lithofacies	Code	Sub-lithofacies	Code	Lithology	Interpretation
Massive sandy conglomerate	Gm	Massive sandy conglomerate, lag deposits	Gml	Fine- to medium-grained sandy conglomerate	Lag deposits at the bottom of channels. Gravel particle size is 0.2−1.5 cm, massive bedding. Formed under strong hydrodynamic conditions (Fig. 3(a)).
		Massive sandy conglomerate, non-lag deposits	Gm2	Fine- to medium-grained sandy conglomerate	Non-lag deposits within channel bar. Gravel particle size is 0.5−1.0 cm, massive bedding or large-scale trough cross-bedding. Formed under strong hydrodynamic conditions (Fig. 3(b)).
Parallel bedded sandstone	Sh	Parallel bedded sandstone	Sh	Medium-to coarse-grained sandstone	Commonly observed in the middle and upper parts of large channels, middle channel bars and side bars. Formed under strong hydrodynamic conditions (Fig. 3(c)).
Trough cross-bedded sandstone	St	Large trough cross-stratification sandstone	St1	Medium-to coarse-grained sandstone	Typical channel deposits, mainly found in the middle and lower parts of large-scale braided channel deposits. Formed under strong hydrodynamic conditions (Fig. 3(d)).
		Small trough cross-stratification sandstone	St2	Medium-to coarse-grained sandstone	Typical channel deposits, mainly found in the middle and lower parts of small-scale braided channel deposits. Formed under relatively weak hydrodynamic conditions than that of St1.
Tabular cross-bedded sandstone	Sp	Large tabular cross-stratification sandstone	Sp1	Medium-to coarse-grained sandstone	Formed in inter-river areas with strong hydrodynamic conditions and open terrain. Mostly observed in the lower to middle parts of the channel bars and side bars and upper parts of large channel deposits (Fig. 3(f)).
		Small tabular cross-stratification sandstone	Sp2	Medium-to coarse-grained sandstone	Formed in inter-river areas with weaker hydrodynamic conditions than that of Sp1. Mostly observed in the middle to upper parts of the channel bars, side bars and affiliation bars and the upper parts of small channel deposits (Fig. 3(g)).
Massive sandstone	Sm	Massive sandstone	Sm	Medium-to coarse-grained sandstone	Formed by the rapid unloading of sediments under strong hydrodynamic conditions, mostly found in the main channel, middle channel bar and side bar deposits (Fig. 3(h)).
Massive mudstone	Mm	Massive mudstone	Mm	Mudstone	Formed on open floodplains with mainly muddy sediments (Fig. 3(i)).

4.6 Massive mudstone

Massive mudstone is mostly formed during the flood events, and its thickness is generally greater than 0.2 m (Fig. 3(i)). The proportion of the lithofacies Mm is relatively low, accounting for less than 10% of the entire outcrop area.

5 Sedimentary architecture elements

Based on the identified lithofacies, the lithofacies association were recognized and the sedimentary architecture elements were further determined on the outcrop. Under the framework of fluvial sedimentary architecture proposed by Miall (1985), we propose a

more detailed classification system for braided river sedimentary architecture. The 5th-3rd level sedimentary architecture elements were recognized based on the lithofacies association, the dimension and inferred relative hydrodynamic strength (Table 2). The 5th-level SAEs in a braided river can be divided into the river bedform and the overbank deposition, and the former is the main body of braided river deposits. The river bedform can be divided into two types of 4th-level SAEs including channel bar and braided channel. According to the differences in sedimentary characteristics, scale and formation mechanism of various 4th-level architecture elements, and on the basis of the above rough classification, these two types of architecture elements were detailed classified (Table 2).

5.1 Braided channels

The braided channel deposits identified on the Tianshengqiao outcrop also show obvious differences in scale, spatial pattern and sedimentary characteristics and can be classified as the main channel, the secondary channel and abandoned channel.

5.1.1 Main channel

According to outcrop analysis, the depth of the main channel is 8−15 m, and the width can reach more than tens of meters (Fig. 4), which is the largest among the three types of channels. The main channel is generally distributed between channel bars, and has a large width and depth (Fig. 5). Strong hydrodynamic force carries most of the sediments during the depositional process. On the vertical direction, there is an obvious fine upward trend of its sediment grain size. The lithofacies types at the bottom of the channel are Gm1 and St2, upwards become Sm and Sh, and the top is generally Sp1 (Fig. 5). Affected by seasonal hydrodynamic fluctuations, the

Table 2 Architecture elements of a braided river

5th-level element	4th-level element		3rd-level element	Thickness/m	Relative hydrodynamic	Lithofacies association
	Rough classification	Detailed classification				
River bedform	Braided channel	Main channel (Chm)	Lateral accretions	8.0−15.0	Very Strong	Gm1, St1, Sm, Sh, Sp1
		Secondary channels (Chs)	Lateral accretions	1.5−5.0	Weak	Gm1, St2, Sp2, Sh
		Abandoned channel (Cha)	Centripetal accretions	1.5−4.0	Weak	Gm1, St2, Sp2, Sh, Mm
	Channel bar	Middle channel bar (Bm)	Downstream accretions	9.0−15.0	Very strong	Gm2, St1, Sp1, Sp2, Sm, Sh
		Side bar (Bs)	Lateral accretions	4.0−10.0	Strong	Gm2, St2, Sp1, Sp2, Sm
		Affiliated bar (Ba)	Lateral accretions	1.5−3.5	Weak	Sp2
Overbank deposition	Overbank deposition	Overbank Deposition (O)	Horizontal accretions	0.2−3.5	Weak	Mm

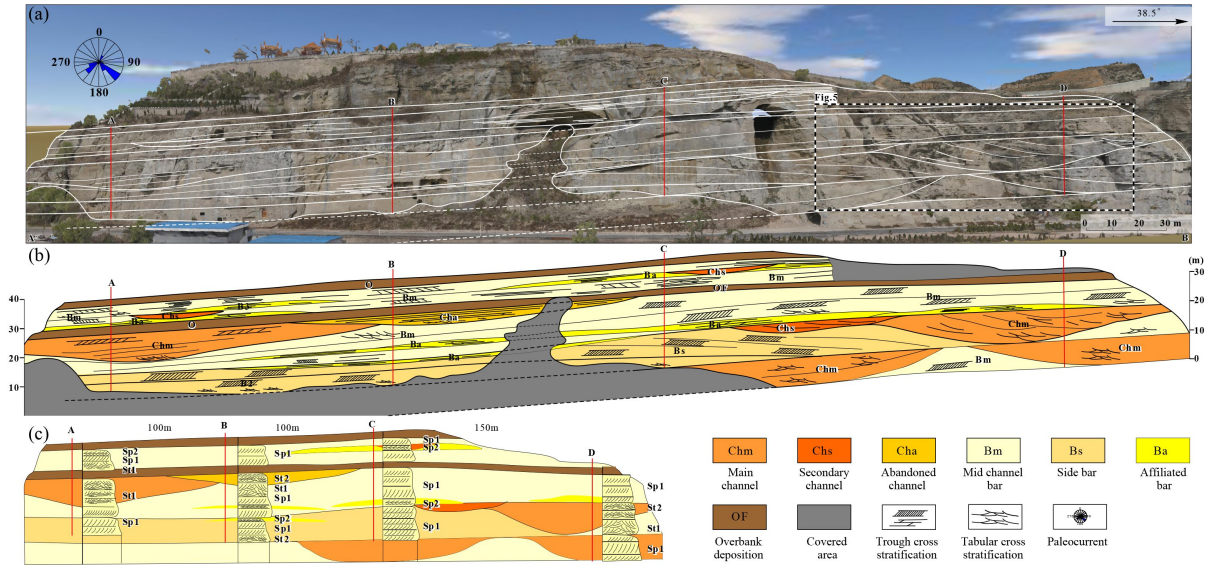

Fig. 4 Sedimentary architecture of the braided river on profile A-B of the Tianshengqiao outcrop, profile location shown in Fig. 1(b). (a) Image and architectural boundaries of profile A–B, (b) sedimentary architecture interpretation of the A–B profile, (c) inferred sedimentary architecture interpretation of the A–B profile.

water level in main channels rises and falls with the change of discharge, which complicates its vertical lithofacies association.

5.1.2 Secondary channel

Compared with the main channel, the secondary channel is smaller in scale but larger in amount, distributed inside channel bars. It is generally 10−30 m wide and 1.5−5 m deep (Fig. 4). Most of the secondary channels originate from the main channel on the upper stream edge of the channel bar, and are formed by the water overflowing to the top of the channel bar (Fig. 6). In a channel bar, multiple secondary channels coexist at the same time. After flowing through the channel bar, the secondary channel finally joins the downstream main channel (Fig. 7). On the vertical direction, there is an obvious fine upward trend of the sediment grain size. The lithofacies types at the bottom of the channel are GM1, upwards become St2 and Sp2, and the top is generally Sh (Fig. 5).

The secondary channels mainly distribute on the top of channel bar, the existence of which requires high water

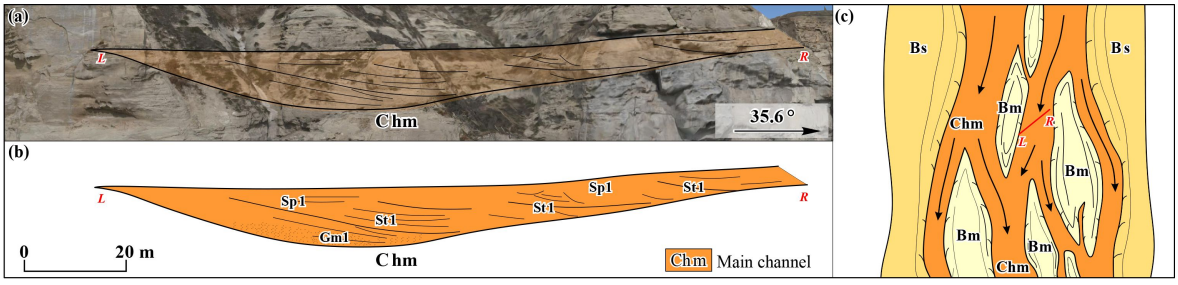

Fig. 5 Sedimentary characteristics of the main channel (Chm). (a) Image of a Chm on the Tianshengqiao outcrop, (b) architecture and lithofacies distribution of the Chm, (c) horizontal architecture of the Chm in a braided river.

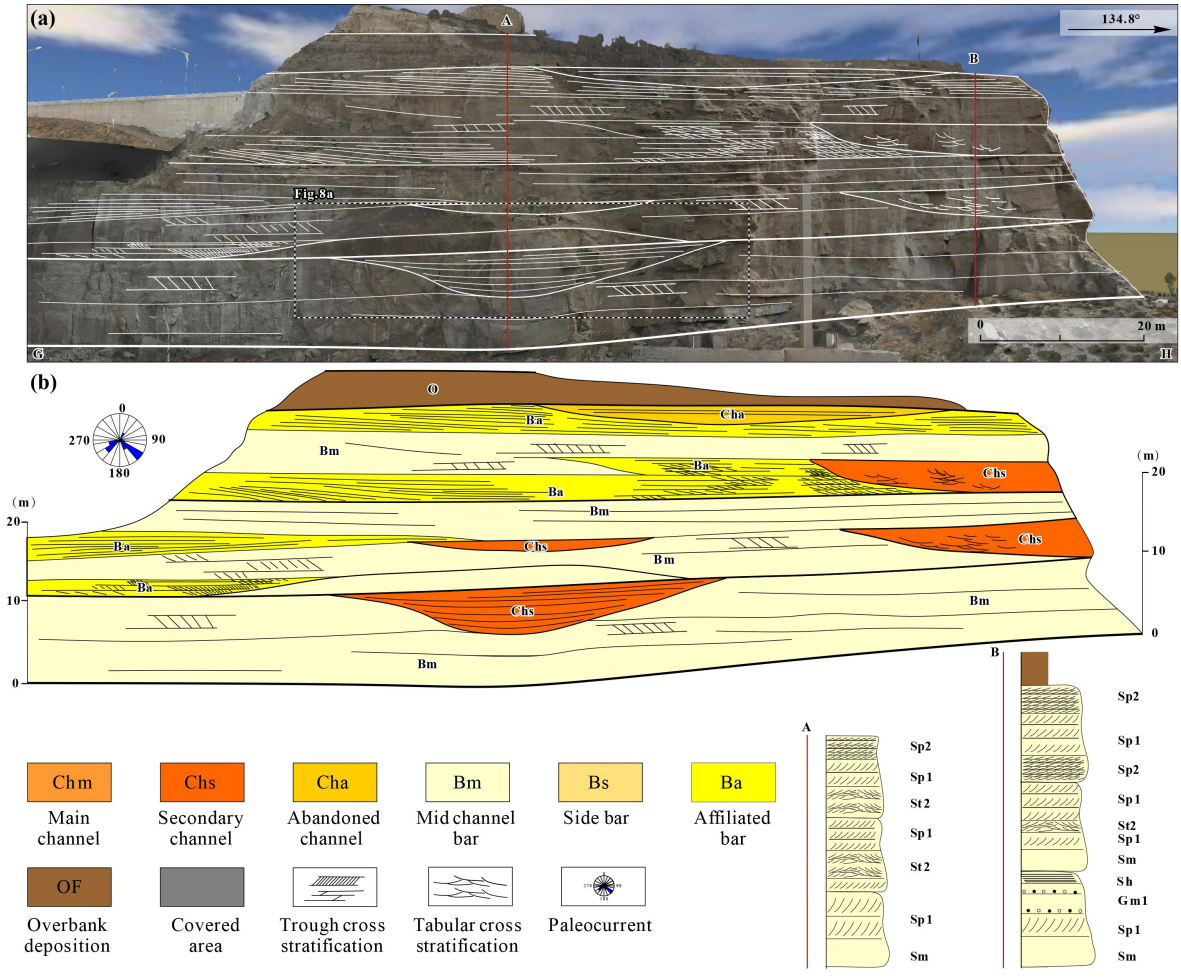

Fig. 6 Sedimentary architecture of the braided river on profile G-H of the Tianshengqiao outcrop, profile location shown in Fig. 1(b). (a) Image and architectural boundaries of profile G-H, (b) sedimentary architecture interpretation of the G-H profile.

levels, and they are usually active in flood seasons. Some secondary channels dry up in normal seasons. (Fig. 6).

5.1.3 Abandoned channel

As observed on the Tianshengqiao outcrop, abandoned channels are relatively rare in braided river deposits (Figs. 4 and 6). Centripetal accretions are the dominant elements within an abandoned channel. From the bottom of the channel to the top, lithofacies changes from Gm1, St2, Sp2, to Sh and finally ended with Mm (Fig. 7). The thickness of the abandoned channel deposit is 1.5−4.0 m, and the width is about 30 m (Fig. 7).

5.2 Channel bars

According to the observation of the Tianshengqiao outcrop, channel bars were recognized and further divided into three types, including mid-channel bar, side bar, and affiliated bar, based on the variations of their scale, geometry, lithofacies association.

5.2.1 Middle channel bar

Bm distributed in the middle belt of the river bed, the middle channel bar, generally irregularly elliptical and surrounded by main channels, is the main body of braided river deposits (Figs. 4 and 6). The middle channel bar is large in scale, with a thickness of 9−15 m and a width of more than hundreds of meters. There are several downstream accretions inside a middle channel bar. Along the longitudinal direction, the accretions present the pattern of progradation, while in the transversal direction, the accretions present the geometry of flat bottom and convex top (Fig. 8). Due to the large size of the middle channel bar, the accretions tend to be relatively flat on the Tianshengqiao outcrop of limited length. As observed on the transversal profile of the Tianshengqiao outcrop, the edge of the middle channel bars was cut by the main channel, while the accretions inside the middle channel bar is observed to coexist with the secondary channels and their subsidiary deposits (Figs. 4 and 6). Driven by various hydrodynamic conditions, various types of lithofacies developed in the channel bank, including Gm2, St2, Sp1, Sp2, Sm, Sh (Figs. 4 and 6).

5.2.2 Side bar

A side bar exists along one bank of a braided river. Only one side of the side bar (Bs) is affected by the main channel, while the other side is connected to the river bank. Since the main braided river channel is mainly distributed near the center line of the river bed and rarely touches the river bank, side bars are often long, but the width is uneven, and most of them are irregular strip-shaped (Fig. 8). Under the influence of the main channel on one side, multiple large-scale lateral accretions develop inside the side bar (Figs. 4 and 8). The thickness of the side dam can reach 4−10 m, and the width can reach more than hundreds of meters (Fig. 4). Vertically, the grain size of the sediment gradually becomes finer from bottom to top, and the lithofacies type changes from Gm2 to St2, Sp1, Sp2, and finally ends with Sm (Fig. 4).

5.2.3 Affiliated bar

According to outcrop observations, the scale of the

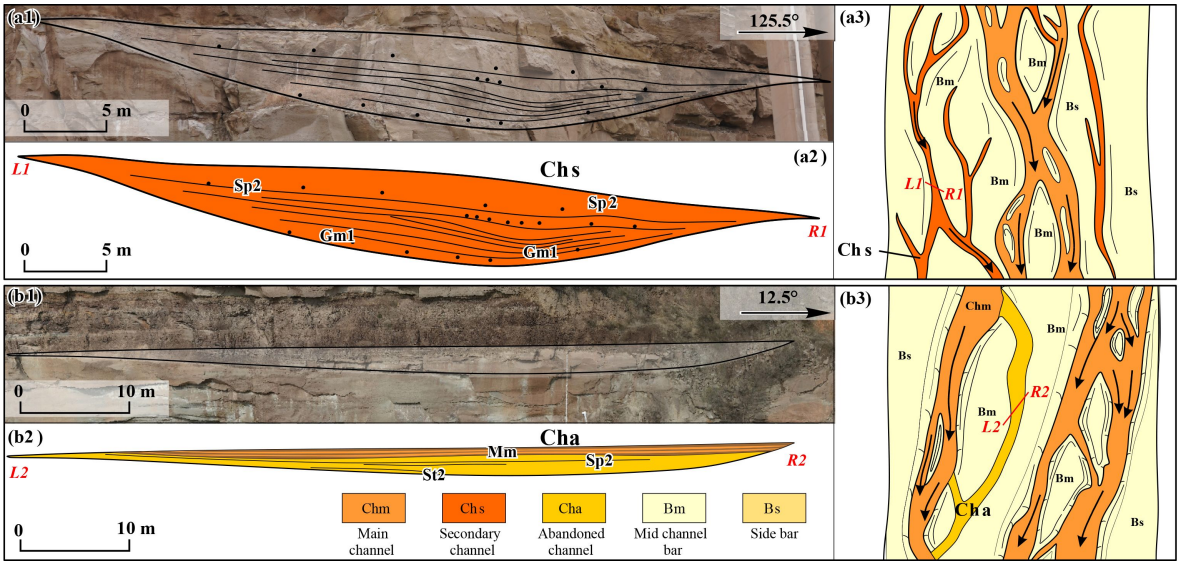

Fig. 7 Sedimentary characteristics of the secondary channel (Chs) and the abandoned channel (Cha). (a1) Image of a Chs on the Tianshengqiao outcrop, (a2) architecture and lithofacies distribution of the Chs, (a3) horizontal architecture of the Chs in a braided river, (b1) image of a Cha on the Tianshengqiao outcrop, (b2) architecture and lithofacies distribution of the Cha, (b3) horizontal architecture of the Cha in a braided river.

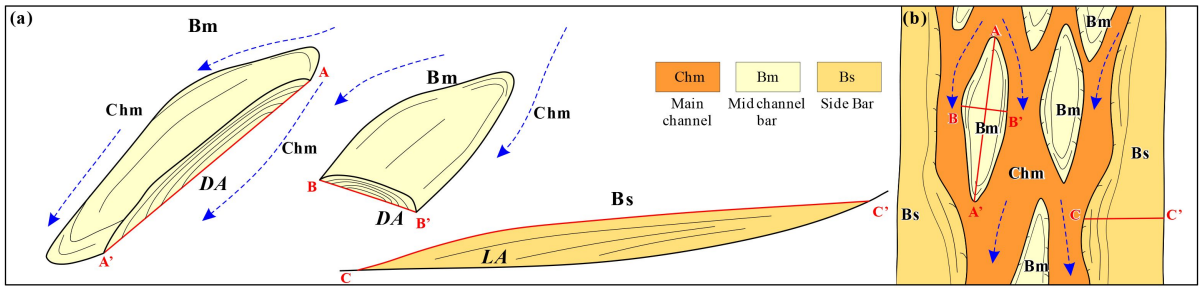

Fig. 8 Sedimentary characteristics of the middle channel bar (Bm) and the side bar (Bs). (a) Architecture of Bm and Bs, (b) horizontal architecture of the Bm and Bs in a braided river.

affiliated bar is smaller than the middle channel bar and the side bar, with a thickness of 1.5−3.5 m and a width of about tens of meters (Figs. 4 and 6). Affiliated bars are generally distributed inside the middle channel bar and the side bar. Due to the small scale of the secondary channel, its influence on the upper part of the middle channel bar or the side bar is limited, and only small-scale affiliated bar can be formed along the flow path of the secondary channels (Figs. 4 and 6). Due to the weak hydrodynamic force of the secondary channel, the sediment grain size of the formed affiliated bar is finer than that of the middle channel bar and the side bar, and the lithofacies is mainly Sp2 (Figs. 4 and 6).

5.3 Overbank deposition

Overbank deposition is formed by the suspended sediments carried by the river when it floods. The main sediments are mud, the typical lithofacies is Mm. The distribution of the overbank deposition depends on the distribution of the floodplain and the intensity of the flood event. On the Tianshengqiao outcrop, the internal lithofacies of the overbank deposits is Mm, with a thickness of 0.2−3.5 m and a maximum width of more than 1 km (Figs. 4 and 6).

6 Discussion

6.1 Sedimentary architecture elements and associated hydrodynamic conditions

Hydrodynamic conditions dominate the formation of lithofacies and architecture elements (Miall, 1985). Controlled by seasonal fluctuations in hydrodynamic conditions, the depositional processes and sediments of braided rivers are significantly different during normal and flood periods. Taking the lithology, sedimentary structure, scale and spatial distribution into consideration, the six types of lithofacies and nine types of sub-lithofacies observed on the outcrop (Table 1) can be classified into two groups. Group 1 includes Gm1, Gm2, Sh, St1, Sp1, and Sm, which are formed under strong hydrodynamic condition. In contrast, Group 2 includes St2, Sp2, and Mm, which are deposited under weaker hydrodynamic conditions.

On the basis of outcrop and modern braided river observations, architecture elements formed under different hydrodynamic conditions were further identified (Table 2). During the flood season, the water level is high, the hydrodynamic force is strong, and the sediment load is high. The main channels and the secondary channels are active at the same time, resulting in the deposition of the accretions in the main channel, the secondary channel, the mid-channel bar, the side bar, and the affiliated bar. It is worth noting that even during the flood period, the hydrodynamic force in the secondary channels is relatively weak. If the water level exceeds the river bank, the overflow bank deposits of the floodplain will still develop. In normal season, as the water level of the river bed decreases, the hydrodynamic force is weak and the sediment load is significantly reduced, and the water level in the main channel is also low. As a result, limited water flow can only reform the deposited sediments and form weak hydrodynamic products in the main channels. At the same time, the secondary channels dry up. Therefore, the main deposition of braided rivers occurred during the flood season, and there were differences in hydrodynamic force and associated depositional characteristics within the riverbed.

6.2 Hydrodynamics dominated channel scale

The scale of a channel is critical to forecasting subsurface channel deposition. Hierarchies of channels in braided rivers have been identified and classified in previous studies using several different schemes (Williams and Rust, 1969; Bridge, 1993). Skelly et al. (2003) observed that channel elements occur on several scales, from the relatively small channels that comprise the braided channel complex at relatively low discharges (i.e., secondary channels) to the single channel present at high discharges (i.e., the main channel). However, it is difficult to determine the extent of the sediment in the braided river from the outcrops. Based on the relationship and empirical equation of the deposit and river channel established by the former authors (Wang and Zhao, 2021), the scale of the channel is reconstructed and

validated with outcrop data. The mean height of the sand dune is calculated from the mean thickness of the cross-stratification, which is given by

$$h_{\mathrm{m}} = 2.22\left(\frac{S_{\mathrm{m}}}{1.8}\right)^{1.32}, \quad (1)$$

where h_{m}, means dune height; S_{m}, means cross-stratification layer thickness.

A statistical relationship between the average bank flow depth and the mean sand dune height was obtained. Its calculation formula is

$$d_{\mathrm{m}} = 6h_{\mathrm{m}}, \quad (2)$$

where d_{m}, the average full bank flow depth of braided channel.

Then, the mean width of the channel was calculated according to the statistical relation of channel width and channel depth. The calculation formula is as follows:

$$w_{\mathrm{c}} = 8.88d_{\mathrm{m}}^{1.82}, \quad (3)$$

where w_{c}, means channel width; d_{m}, means channel depth.

Finally, the width of the braided stream is calculated based on the relation between the width of the braided stream and the mean depth of the whole bank. Its calculation formula is

$$Ch_{\mathrm{w}} = 59.9d_{\mathrm{m}}^{1.8}, \quad (4)$$

where Ch_{w}, the width of a braided stream; d_{m}, the mean full bank depth of a single channel.

Based on the above calculations, the width of the braided channel and the width of the channel belt were calculated (Table 3).

Through the measurement of cross-layer thickness in 3D digital outcrops, the width of the braided channel and braided stream in the He 8 section was calculated, and the results showed that there were two kinds of braided channels in the channel belt. The width of the large-scale channel with high energy is 45.6−764.5 m, and the width of the channel belt is 301.8−4929.6 m. The width of the small-scale channel with low energy is 2.5−26.7 m, and the width of the channel belt is 17.3−177.6 m. The result of the prediction agrees with the real parameters of the outcrop.

6.3 Sedimentary architecture model

Based on the practical observation of the outcrops, the basic spatial patterns of the typical architecture elements of the outcrop have been established. The spatial patterns suggest that architecture elements formed under different hydrodynamics may be combined in the same depositional environment (Fig. 9).

There are two main types of architecture element combinations including strong hydrodynamic combination and weak hydrodynamic combination. The strong hydrodynamic combination formed in flood periods, including the main braided channels, middle channel bar, and side bar (Fig. 9). The weak hydrodynamic combination includes secondary braided channels, abandoned channels, and affiliated bars (Fig. 9). Even in the flood periods, there is a significant difference in hydrodynamics between the main braided channel and the secondary braided channel. The secondary braided channels and associated affiliated bars are classified as a weak hydrodynamic combination.

The outcrop is mainly made up of strong hydrodynamic combinations, and weak hydrodynamic combinations are mainly located on the upper part of the strong hydrodynamic combinations. In the long term sedimentation process, strong water flow during the flood period continuously erodes pre-existing sediments and forms new sediments, while weak water flow during the normal period can only reform the main braided channels and their adjacent channel bar sediments. Therefore, regardless of seasonal hydrodynamic changes, the main body of braided river sediments is a collection of strong hydrodynamic combinations (Fig. 10).

7 Conclusions

Nine lithofacies including Ge, Gm, Sh, St1, St2, Sp1, Sp2, Sm, and Mm were identified by the digital outcrop model. Based on the identification and classification of the lithofacies, seven architecture elements have been recognized including Chm, Chs, Cha, Bm, Bs, Ba, and OF.

Based on the lithofacies and inferred hydrodynamics, the sedimentary process of seasonal hydrodynamic variation dominated braided river was established. During the flood period, the main braided channels surrounding channel bars and the secondary braided channels distributed on the top of the channel bars coexisted, forming a highly braided channel network. Migration of the main braided channels controlled the formation of

Table 3 Quantified geometric properties of the sandy braided river from He8 outcrops in the study area

Type	Channel width/m			Channel belt width/m		
	Max	Min	Avg	Max	Min	Avg
High energy channel	764.5	45.6	206.5	4929.6	301.8	1345.7
Low energy channel	26.7	2.5	8.5	177.6	17.3	57.1

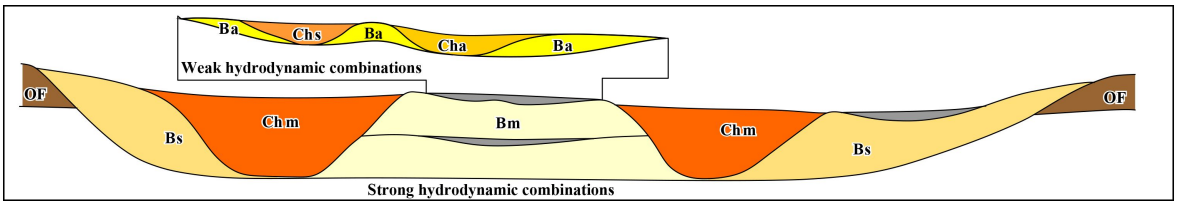

Fig. 9 Schematic diagram of the architecture element combinations. Combination under strong hydrodynamics in flood periods, occupying more than 90% of the braided river. It contains the following elements: Bm, Bs, CHm, and OF (OF is concomitant with strong hydrodynamics when flowing over the bank, not formed in it). Combination under weak hydrodynamics occurring at the tops of unit bars (Bm or Bs). It contains the following elements: CHs, CHa, and Ba.

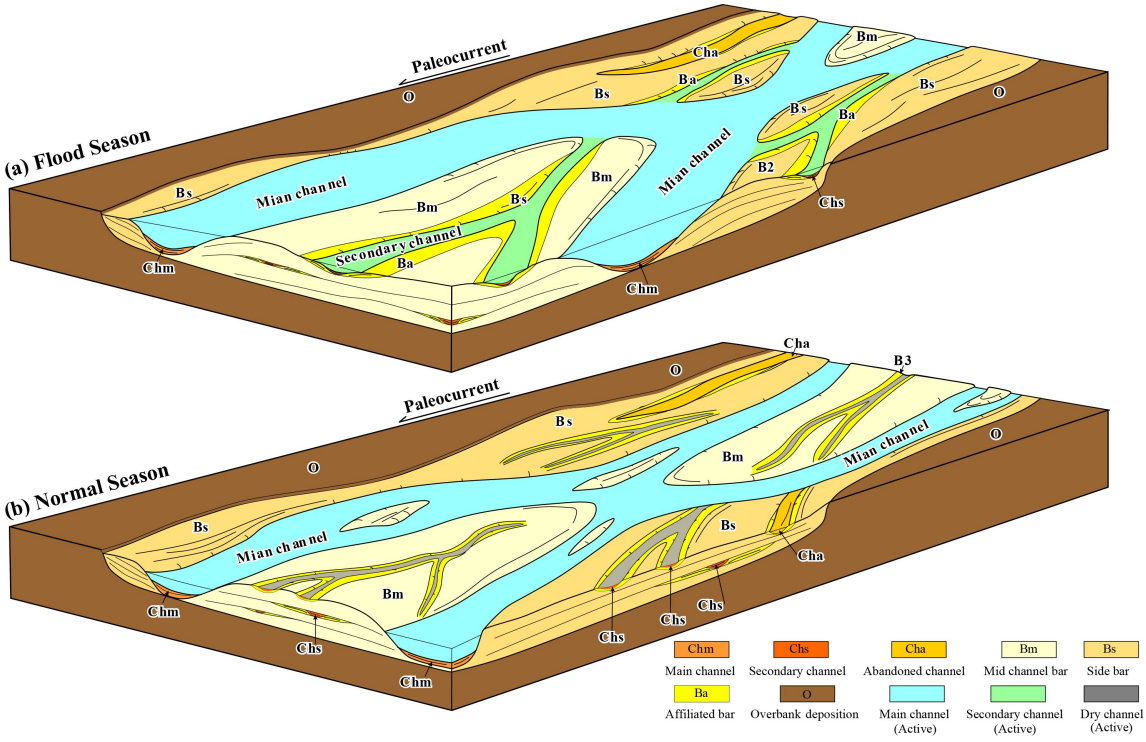

Fig. 10 The sedimentary architecture model and flow pattern of a sandy braided river in flood and normal season. (a) sedimentary architecture and flow pattern in flood season, (b) sedimentary architecture and flow pattern in flood season.

middle channel bars and side bars. The generation and evolution of the secondary braided channels reformed the upper part of preexist channel bars and produced affiliated bars along their flow path. During the normal period, the water level decreases, causing the secondary river channels to be abandoned and formed abandoned channels, while only the main braided channels still stay active.

Based on differences in sedimentary process and associated hydrodynamic conditions, we divide braided river sediments into two combinations. The strong hydrodynamic combination includes the main braided channels, middle channel bar, and side bar, while the weak hydrodynamic combination includes secondary braided channels, abandoned channels, and affiliated bars. Among them, the proportion of strong hydrodynamic combinations is much larger than that of weak hydrodynamic combinations.

Competing interests The authors declare that they have no competing interests.

References

Allen J R L (1983). Studies in fluviatile sedimentation: bars, bar-complexes and sandstone sheets (low-sinuosity braided streams) in the Brownstones (L. Devonian), Welsh Borders. Sediment Geol, 33(4): 237–293

Ashmore P (1991). Channel morphology and bed load pulses in braided, gravel-bed streams. Geogr Ann, Ser A, 73(1): 37–52

Ashmore P E (1982). Laboratory modelling of gravel braided stream morphology. Earth Surf Process Landf, 7(3): 201–225

Ashworth P J, Best J L, Roden J E, Bristow C S, Klaassen G J (2000). Morphological evolution and dynamics of a large, sand braid-bar, Jamuna River, Bangladesh. Sedimentology, 47(3): 533–555

Best J L, Ashworth P J, Bristow C S, Roden J (2003). Three-dimensional sedimentary architecture of a large, mid-channel sand

braid bar, Jamuna River, Bangladesh. J Sediment Res, 73(4): 516–530

Blodgett R H, Stanley K O (1980). Stratification, bedforms, and discharge relations of the Platte braided river system, Nebraska. J Sediment Res, 50(1): 139–148

Bluck B J (1979). Structure of coarse grained braided stream alluvium. Earth Environ Sci Trans R Soc Edinb, 70(10−12): 181–221

Bridge J S (1993). The interaction between channel geometry, water flow, sediment transport and deposition in braided rivers. Spec Publ Geol Soc Lond, 75(1): 13–71

Bridge J S (2003). Rivers and Floodplains: Forms, Processes, and Sedimentary Record. New York: John Wiley & Sons

Bridge J S, Smith N D, Trent F, Gabel S L, Bernstein P (1986). Sedimentology and morphology of a low-sinuosity river: Calamus River, Nebraska Sand Hills. Sedimentology, 33(6): 851–870

Bridge J S, Tye R S (2000). Interpreting the dimensions of ancient fluvial channel bars, channels, and channel belts from wireline-logs and cores. AAPG Bull, 84(8): 1205–1228

Bristow C S (1987). Brahmaputra River: channel migration and deposition. Recent Develop Fluvial Sediment, 39: 63–74

Cain S A, Mountney N P (2009). Spatial and temporal evolution of a terminal fluvial fan system: the Permian Organ Rock Formation, South-east Utah, USA. Sedimentology, 56(6): 1774–1800

Cant D J, Walker R G (1978). Fluvial processes and facies sequences in the sandy braided South Saskatchewan River, Canada. Sedimentology, 25(5): 625–648

Carson M A (1984). The meandering-braided river threshold: a reappraisal. J Hydrol (Amst), 73(3−4): 315–334

Chen D, Wang F, Chen H, Wei X, Sun S, Zhu S (2019). Characterization of braided river reservoir architecture of the Upper Paleozoic He 8 member on Fugu Tianshengqiao outcrop, eastern Ordos Basin. Oil Gas Geol, 40: 335–345

Chen Q, Li W, Liu H, Li K, Pang J, Guo Y, Yuan Z (2009). Provenance analysis of sandstone of the Upper Carboniferous to Middle Permian in Ordos Basin. J Palaeogeogr, 11(6): 629–640 (in Chinese)

Coleman J M (1969). Brahmaputra River: channel processes and sedimentation. Sediment Geol, 3(2−3): 129–239

Collinson J D (1970). Bedforms of the Tana river, Norway. Geogr Ann, Ser A, 52(1): 31–56

Doeglas D J (1962). The structure of sedimentary deposits of braided rivers. Sedimentology, 1(3): 167–190

Fielding C R, Alexander J, Allen J P (2018). The role of discharge variability in the formation and preservation of alluvial sediment bodies. Sediment Geol, 365(MAR): 1–20

Fielding C R, Allen J P, Alexander J, Gibling M R (2009). Facies model for fluvial systems in the seasonal tropics and subtropics. Geology, 37(7): 623–626

Gao P, Li Z, You Y, Zhou Y, Piégay H (2022). Assessing functional characteristics of a braided river in the Qinghai-Tibet Plateau, China. Geomorphology, 403: 108180

Gupta A, Dutt A (1989). The Auranga: description of a tropical monsoon river. Z Geomorphol, 33(1): 73–92

Krigström A (1962). Geomorphological studies of sandur plains and their braided rivers in Iceland. Geogr Ann, 44(3−4): 328–346

Li W, Qian Z, Li K, Chen Q, Guo Y, Ma Y, Feng J, Zhang D (2021). Sedimentary evolution of the late Paleozoicin Ordos Basin and its adjacent areas. J Palaeogeogr, 23(1): 39–52 (in Chinese)

Li Z, Lu H, Gao P, You Y, Hu X (2020). Characterizing braided rivers in two nested watersheds in the source region of the Yangtze River on the Qinghai-Tibet Plateau. Geomorphology, 351: 106945

Miall A D (1977a). A review of the braided-river depositional environment. Earth Sci Rev, 13(1): 1–62

Miall A D (1977b). Lithofacies types and vertical profile models in braided river deposits: a summary. Fluvial Sedimentology. Memoir 5: 597–604

Miall A D (1985). Architectural-element analysis: a new method of facies analysis applied to fluvial deposits. Earth Sci Rev, 22(4): 261–308

Miall A D (2013). The Geology of Fluvial Deposits: Sedimentary Facies, Basin Analysis, and Petroleum Geology. New York Springer

Mosley M P (1983). Response of braided rivers to changing discharge. J Hydrol NZ, 22(1): 18–67

Plink-Björklund P (2015). Morphodynamics of rivers strongly affected by monsoon precipitation: review of depositional style and forcing factors. Sediment Geol, 323: 110–147

Skelly R L, Bristow C S, Ethridge F G (2003). Architecture of channel-belt deposits in an aggrading shallow sandbed braided river: the lower Niobrara River, northeast Nebraska. Sediment Geol, 158(3−4): 249–270

Smith N D (1970). The braided stream depositional environment: comparison of the Platte River with some Silurian clastic rocks, north-central Appalachians. Geol Soc Am Bull, 81(10): 2993–3014

Smith N D (1974). Sedimentology and bar formation in the upper Kicking Horse River, a braided outwash stream. J Geol, 82(2): 205–223

Vandenberghe J (1995). Timescales, climate and river development. Quat Sci Rev, 14(6): 631–638

Wang A Q, Su B D, Huang J L, Jing C, Kundzewicz Z W, Tao H, Zhan M, Jiang T (2023). Runoff components and the contributions of precipitation and temperature in a highly glacierized river basin in Central Asia. Front Earth Sci, 17(2): 361–377

Wang K, Zhao J F (2021). Fluvial sedimentary types and their evolution in the Yan'an Formation in the Ordos Basin: evidence from the detailed anatomy of typical outcrops. Acta Sediment Sin, 1: 1–13

Wen H, Zheng R, Gao H, Dai Z, Li G (2007). Sedimentary facies of the 8th member of lower Shihezi Formation in Su6 area, Sulige Gas Field. Acta Sediment Sin, 25(1): 90–98 (in Chinese)

Williams P F, Rust B R (1969). The sedimentology of a braided river. J Sediment Res, 39(2): 649–670

Yang R, Han Z, Li W, Fan A, Li Y (2004). Sedimentary characteristics and models of deltas from Permian system in Ordos area. J Northwest U (Nat Sci edition), 34(3): 340–344 (in Chinese)

You Y, Li Z, Gao P, Hu T (2022). Impacts of dams and land-use changes on hydromorphology of braided channels in the Lhasa River of the Qinghai-Tibet Plateau, China. Int J Sediment Res, 37(2): 214–228